Research Article

Hongcai Li#, Tinghua Li#, Qian Wu, Rui Wang, Ruoyu Hong*, and Yonggang Li*

Super stable water-based magnetic fluid as a dual-mode contrast agent

https://doi.org/10.1515/ntrev-2021-0068
received May 06, 2021; accepted July 16, 2021

Abstract: Early diagnosis of cancer has become one of the effective ways to prevent and treat cancer. At present, magnetic resonance imaging (MRI) diagnosis based on nanosized iron oxide with no toxicity and excellent biocompatibility has attracted much attention. But the poor stability of magnetic fluid (MF) is becoming more and more prominent. In view of the poor stability of MF, the dodecanethiol-poly(methacrylic acid) (DDT-PMAA) as an outer shell was prepared for the MFs (Fe_3O_4@DDT-PMAA MF) to improve the stability. We also compared the amount of reactants, the ratio of reactants, and the reaction temperature, and finally screened out the best reaction conditions, so as to get more stable products. The stability of the system was studied by visual observation, stability index (I), and magnetic weight change. The results demonstrated that Fe_3O_4@DDT-PMAA can be stable for more than 60 days. The T_1 mapping image showed that the longitudinal relaxivity (r_1) value was 6.9 $mM^{-1}\,s^{-1}$ (1.5 T, room temperature), which was higher than the commercial contrast agent SHU-555 ($r_1 = 2.9\ mM^{-1}\,s^{-1}$), but the transverse relaxivity (r_2) value accounted for 64.48% of the commercial contrast agent Feridex ($r_2 = 67.8\ mM^{-1}\,s^{-1}$, 1.5 T, room temperature) because the outermost layer was encapsulated by a polymer. In addition, the imaging effect was more vivid and there was almost no background interference of T_1- and T_2-weighted images *in vivo*, which indicated that the Fe_3O_4@DDT-PMAA MF exhibited excellent potential in MRI applications.

Keywords: MRI, MF, optimum reaction conditions, stability, dual-model image

1 Introduction

At present, cancer is still one of the diseases that cannot be overcome completely. Therefore, the early diagnosis of cancer is very important for its treatment[1]. Magnetic resonance imaging (MRI) is a very effective test method. Compared with CT and X-ray imaging, MRI has no radiation damage and has high soft tissue resolution, which can be applied to diagnose a variety of tumors [2]. However, conventional MRI contrast agent such as gadolinium (Gd) reagent is expensive and owns certain nephrotoxicity, which fails to use as a diagnostic drug over a long time [3]. Therefore, it is imperative to develop new contrast agents with good imaging effect and excellent biocompatibility, especially with long-term stability [4].

The imaging effect of contrast agents is determined by spin lattice relaxation which is the energy loss of protons from the excited state to the initial state [5]. Spin relaxation is due to the loss of phase coherence in the treatment of protons. The relaxation times and relaxivities are T_1, T_2 and r_1, r_2, respectively [6]. According to these parameters, the contrast agents are usually classified as T_1 positive contrast agents (longitudinal relaxation) with similar r_1 and r_2 values and smaller r_2/r_1, and T_2 negative contrast agents (transverse relaxation) whose r_2 values are much higher than r_1 [7]. At present, the T_1 contrast agent widely used in clinic is Gd-based contrast agent. Because of the strong paramagnetism of Gd^{3+}, the traditional Gd-positive contrast agent, such as divinyltriaminopentanoic acid, has been widely used, which exhibits great enhancement effect in MRI [8]. However, it has a risk of inducing nephrogenic systemic fibrosis for patients with impaired renal function, especially in the elderly [9]. The bright visual field of T_1 contrast medium plays an auxiliary role in accurate diagnosis; therefore,

# These authors contributed equally to this paper.

*** Corresponding author: Ruoyu Hong,** College of Chemical Engineering, Fuzhou University, Fuzhou, Fujian, 350108, China, e-mail: rhong@fzu.edu.cn
*** Corresponding author: Yonggang Li,** Medical College, Soochow University, Suzhou, Jiansu, 215006, China, e-mail: liyonggang224@163.com
Hongcai Li, Tinghua Li, Qian Wu: College of Chemical Engineering, Fuzhou University, Fuzhou, Fujian, 350108, China
Rui Wang: Medical College, Soochow University, Suzhou, Jiansu, 215006, China

the development of alternative T_1 contrast agent has always been a hot issue. MnO and FeCo nanoparticles (NPs) show great potential in this respect [10]. But, the cumulative toxicity of manganese and cobalt may limit their clinical application. Iron is an essential component of human cells, so ferrite magnetic NPs with extremely low biotoxicity have been favored in clinical practice [11]. But at present, ferrite is mainly used as T_2 contrast agent because of the strong magnetic moment effect of Fe; however, the dark field produced by T_2 contrast agent is easy to be confused with tissue, which is the inherent defect of the contrast agent [12]. Therefore, it is necessary to solve those problems in order to use ferrite NPs as a contrast agent for T_1- and T_2-weighted MRI [13]. Reducing the particle size of the magnetic NPs is a useful method [14]. Super-small magnetic NPs have obvious longitudinal relaxation and small ratio of r_2/r_1, which indicates that they have great potential as T_1-positive and T_2 -negative contrast agents, attracting more and more attention [15]. At present, the preparation of super-small NPs mainly includes high temperature thermal decomposition method, chemical co-precipitation method, and so on [16]. The Hyeon team [17] prepared ultrasmall NPs with 1.5–3 nm modified with polyethylene glycol by high temperature thermal decomposition which can improve its hydrophilicity. Generally speaking, chemical co-precipitation is more economical than thermal decomposition, and it can be used to prepare water-based magnetic fluid (MF); however, the particle separation is required to prepare monodisperse NPs [18]. Therefore, it is necessary to develop a simple, economical, and environmental friendly method to prepare water-based MF with good dispersion, uniformity, super-small particles, and superparamagnetism. High temperature chemical co-precipitation can be considered as a good choice to obtain small particle, which can be dispersed in water [19]; however, it is crucial to choose the suitable surfactants. Multifunctional polymer ligands play an important role in the process of chemical co-precipitation. Because polymer ligands contain at least one functional group, such as –COOH, –OH, $–NH_2$, and so on, it can effectively control the morphology and particle size of NPs [20]. The presence of polymer ligands not only makes NPs disperse stably in water, but also provides abundant surface functional groups, which lays a good foundation for its surface modification and biological application [21].

In the present investigation, a facile chemical method has been developed to anchor dodecanethiol-poly(methacrylic acid) (DDT-PMAA) on the surface of magnetic NPs in the MF. Because there are several carboxyl groups on the surface of DDT-PMAA functionalized magnetic NPs, the NPs have good stability and water solubility [22]. It is the objective to obtain stable and innoxious water-based MF with super-small NPs, which is considered as a MRI contrast agent for relevant biomedical applications [23]. Therefore, DDT-PMAA with good biocompatibility was selected as the outer layer to improve the stability of MF and reduce the cytotoxicity. The effects of different mass ratios of DDT-PMAA to Fe_3O_4 and different temperatures on the particle size and morphology were studied in detail. The obtained Fe_3O_4@DDT-PMAA MFs was characterized, whose imaging property was researched. In addition, its stability in different environments and storage stability were also studied detailedly.

2 Experimental methods

2.1 Materials

All chemicals were of analytical grade and were used without further purification. Iron(III) chloride hexahydrate ($FeCl_3{\cdot}6H_2O$), iron(II) sulfate heptahydrate ($FeSO_4{\cdot}7H_2O$), aqueous ammonia (25 wt%), methacrylic acid (MAA), 1-dodecanethiol, 2,2′-azobisobis-butyronitrile (AIBN), concentrated hydrochloric acid, anhydrous ether, and absolute ethyl alcohol were all purchased from Sinopharm Chemical Reagent Co., Ltd. (SCRC). The VX2 hepatoma cells were purchased from Cobioer Biotechnology Co., Ltd. (Nanjing, China). Deionized water was used throughout the experiments.

2.2 Characterizations

Transmission electron microscopy (TEM) imaging was performed using a SU8010 ESEM Hitachi microscope (Hitachi, Japan) and a JEM 2100 F, JEOL, Japan, operating at 8.0 and 200 kV, respectively. Fourier transform infrared spectroscopy (FTIR) using Thermo Nicolet 670 FTIR instrument (Thermo Nicolet Corporation, USA) was employed to evaluate the success of functionalization operating at the wavelength range of 4,000–400 cm^{-1}. Raman spectrum was characterized by Raman spectrometer model LabRam HR Evolution with a wavelength range of 200–1,000 cm^{-1} and a laser of 532 nm (HACH, USA). The hydrodynamic particle size and *zeta* potential were measured by Malvern (II) laser particle size analyzer (Malvern, UK). Thermogravimetric analysis (TGA) was carried out by synchronous thermal analyzer (STA449C/6/G, Germany). The valence states between iron and oxygen were measured by X-ray photoelectron spectroscopy (XPS, ESCALAB 250, USA). Magnetic stability

evaluation was performed on the Gouy magnetic balance at room temperature with 25 mT (CTP-II, China). The magnetization of the magnetic NPs was obtained by vibrating sample magnetometer (VSM-7400, Lake Shore, USA). MRI was performed in 3.0 T superconducting magnetic resonance instrument (SIEMENS Skyra, Germany)

2.3 Preparation of DDT-PMAA-modified MF

The DDT-PMAA-modified MF was prepared by high temperature chemical co-precipitation method. First, the synthesis of polymer DDT-PMAA was based on the method reported in the literature [24]. Chain transfer method was used to prepare polymer DDT-PMAA, taking the preparation of 1% of DDT-PMAA as an example, the details were as follows: MAA (5 g, 0.058 mol), 1-dodecanethiol (0.12 g, 0.58 mmol), and AIBN (0.095 g, 0.58 mmol) were dissolved in a 100 mL two neck flask containing 25 mL of anhydrous ethanol at 75°C under magnetic stirring for 5 h. After cooling to room temperature, the solution was poured into a beaker containing 200 mL of cold anhydrous ether to precipitate, filtered, washed the filtered cake with ether, and finally dried to obtain 1% of DDT-PMAA.

Subsequently, polymer DDT-PMAA can be used as a surfactant to prepare MF with super-small particle size by chemical co-precipitation at high temperature. Polymer DDT-PMAA was added into a four-necked flask containing deionized water with slow stirring, raising the temperature to 80°C, and adding hydrochloric acid to adjust the pH of the solution to 4. After the polymer DDT-PMAA was dissolved by stirring slowly, the solution was raised to a certain temperature (95–115°C) and the iron salt precursor (iron(III) chloride hexahydrate and iron(II) sulfate heptahydrate with a molar ratio of 2:1 was dissolved in dilute hydrochloric acid) was added. A certain amount of ammonia solution ($NH_3{\cdot}H_2O$:Fe^{2+} = 1:1.2, mol:mol) was rapidly poured into the four-necked bottle with vigorous stirring, and the color of the solution became black immediately, and continually reacted for 2 h under the same temperature. All processes of the reaction were carried out under the protection of nitrogen. The black suspension was stirred slowly and cooled at room temperature, and some of the unreacted ammonia was vaporized with a rotating evaporator. The residual suspension was dialyzed with deionized water for 72 h to remove unreacted impurity ions. Finally, stable Fe_3O_4 MF modified by polymer DDT-PMAA was obtained.

2.4 Formation process of DDT-PMAA-modified MF

The preparation process of polymer DDT-PMAA-modified Fe_3O_4 MF is shown in Scheme 1. Polymerization of MAA was initiated by chain initiator DDT to form polymer DDT-PMAA [21]. The surface of DDT-PMAA contained a lot of –COOH which can combine with –OH on the surface of Fe_3O_4 NPs to form the stable coordination bonds [21,25]. So, DDT-PMAA can be stably coated on the surface of Fe_3O_4 NPs.

2.5 MRI characterization

2.5.1 *In vitro*

The Fe_3O_4@DDT-PMAA MFs of different concentrations from 0–2.7 mM according to the Fe contents (determined by thermogravimetric analysis) were, respectively, placed in 2.0 mL of sealed EP tubes. The EP tubes were fixed on the plastic plate with holes after shaking with an equal amount of distilled water (0 mg L^{-1} of iron). And the EP tubes were immersed in plastic rectangular containers filled with water.

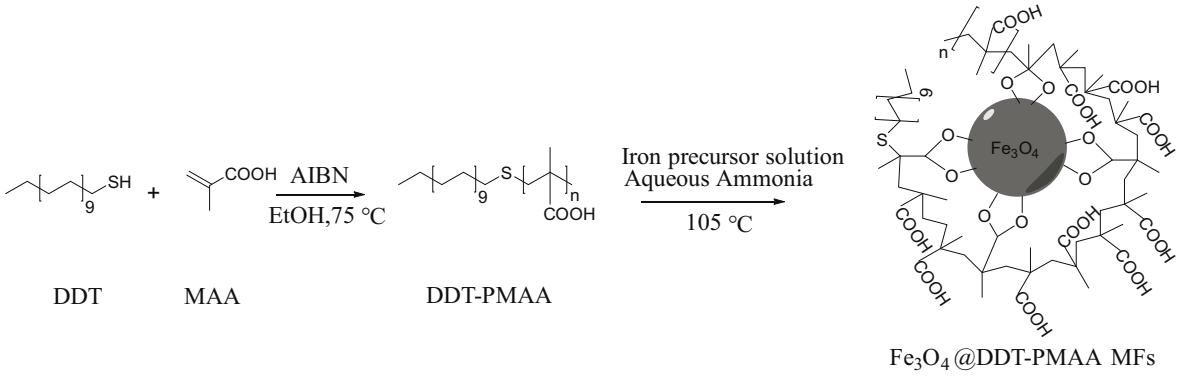

Scheme 1: Schematic illustration of the preparation of DDT-PMAA-modified Fe_3O_4 MFs.

Axis 2D multi-slice MR imaging was performed: field of view was 18 × 18, slice thickness was 2.0 mm, slice spacing was 0 mm, and reconstruction matrix was 256 × 192. The scanning sequences were FSE T_1WI, GRE T_1 map (TE 15 ms, TR 2.29 ms FIIP angle 5°), FSE T_2WI, 4,090 ms, 94 ms, and T_2 map (TR 1,950 ms, TE 13.8 ms).

2.5.2 *In vivo*

Healthy New Zealand male rabbits weighing 2.5 ± 0.5 kg were fed in cages with normal pellet feed at room temperature of 20°C. The VX2 hepatoma cells were injected into healthy rabbits to establish a hepatoma model. Then, the ear veins of every rabbit with VX2 liver cancer were manually pushed into the same concentration of superparamagnetic nano-iron oxide MF, and the signal intensity was enhanced with T_1WI and T_2 WI (dose 4 mL kg^{-1} body weight). USPIO-enhanced scanning was performed by sequential and conventional scanning. Siemens 3.0 abdominal orthogonal coil, scanning sequence and parameter axis spin echo T_1WI sequence, T_2 WI coronal position: TR 3,950, TE 100, Fov read 230 mm, Fov phase 100%, slices 25, and slice thickness 4.0 mm. T_1WI GRE transverse position: TR 3.11 ms, TE 1.68 ms. T_2 map: TR 1,950 ms, TE 13.8 ms.

Scanning range includes the upper and lower edges of the whole liver.

3 Results and discussion

3.1 Influencing factors on particle size of Fe_3O_4@DDT-PMAA MFs

There were many factors, for example, molar ratio between chain initiator DDT and MAA, the dosage of DDT-PMAA, and reaction temperature that would influence the particle size, which determined the effect of T_1 and T_2 signals of MRI. The particle size must be controlled to be small enough to decrease the magnetic moment effect.

3.1.1 The influence of molar ratio between DDT and MAA

Polymer DDT-PMAA was synthesized by DDT and MAA with different molar ratios (0.5, 1, and 2%). The control variable method was used to investigate the effect of 0.5% of DDT-PMAA, 1% of DDT-PMAA, and 2% of DDT-PMAA on the particle size of the NPs. The mass ratio of DDT-PMAA and the obtained Fe_3O_4 was 20:1 and then these reactants reacted at 105°C for 2 h. The hydrodynamic diameter distribution and TEM images are shown in Figures 1 and 2, respectively.

The hydrodynamic diameter distributions of the NPs obtained by the laser particle size analyzer (DLS) show that the particle distribution of Fe_3O_4 MF modified by polymer DDT-PMAA with three different ratios were different (Figure 1). The magnetic NPs prepared with 0.5% of DDT-PMAA had a relatively small particle size, with an average hydrodynamic diameter of only 32.0 nm (PDI = 0.28), and a narrow distribution. The average hydrodynamic diameter of the NPs obtained by 1% of DDT-PMAA was 48.1 nm (PDI = 0.30), and that of 2% of DDT-PMAA reached 37.5 nm (PDI = 0.20).

It can be seen from Figure 2 that the average particle diameter of Fe_3O_4 magnetic NPs modified by 0.5% of DDT-PMAA was 5.9 ± 1.2 nm. The shape of the NPs can be considered as regular sphere with clear edges and an excellent dispersion, which had very little agglomeration. Magnetic NPs modified by 1% of DDT-PMAA and 2% of DDT-PMAA showed similar results, and the average particle size was 10.4 ± 2.1 and 9.4 ± 3.4 nm, respectively. It can be observed that the hydrodynamic diameter obtained by DLS measurement was generally larger than the primary particle size of the MF obtained by TEM, because a large amount of hydrated polymer ligand existed on the surface of the

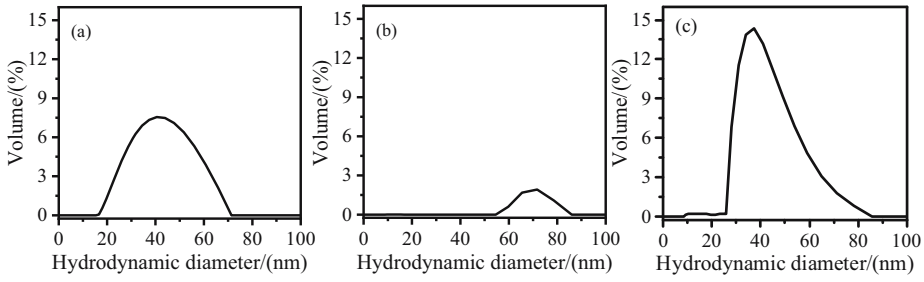

Figure 1: The hydrodynamic diameter distribution of the magnetic NPs at (a) 0.5% of DDT-PMAA; (b) 1% of DDT-PMAA; and (c) 2% of DDT-PMAA, respectively.

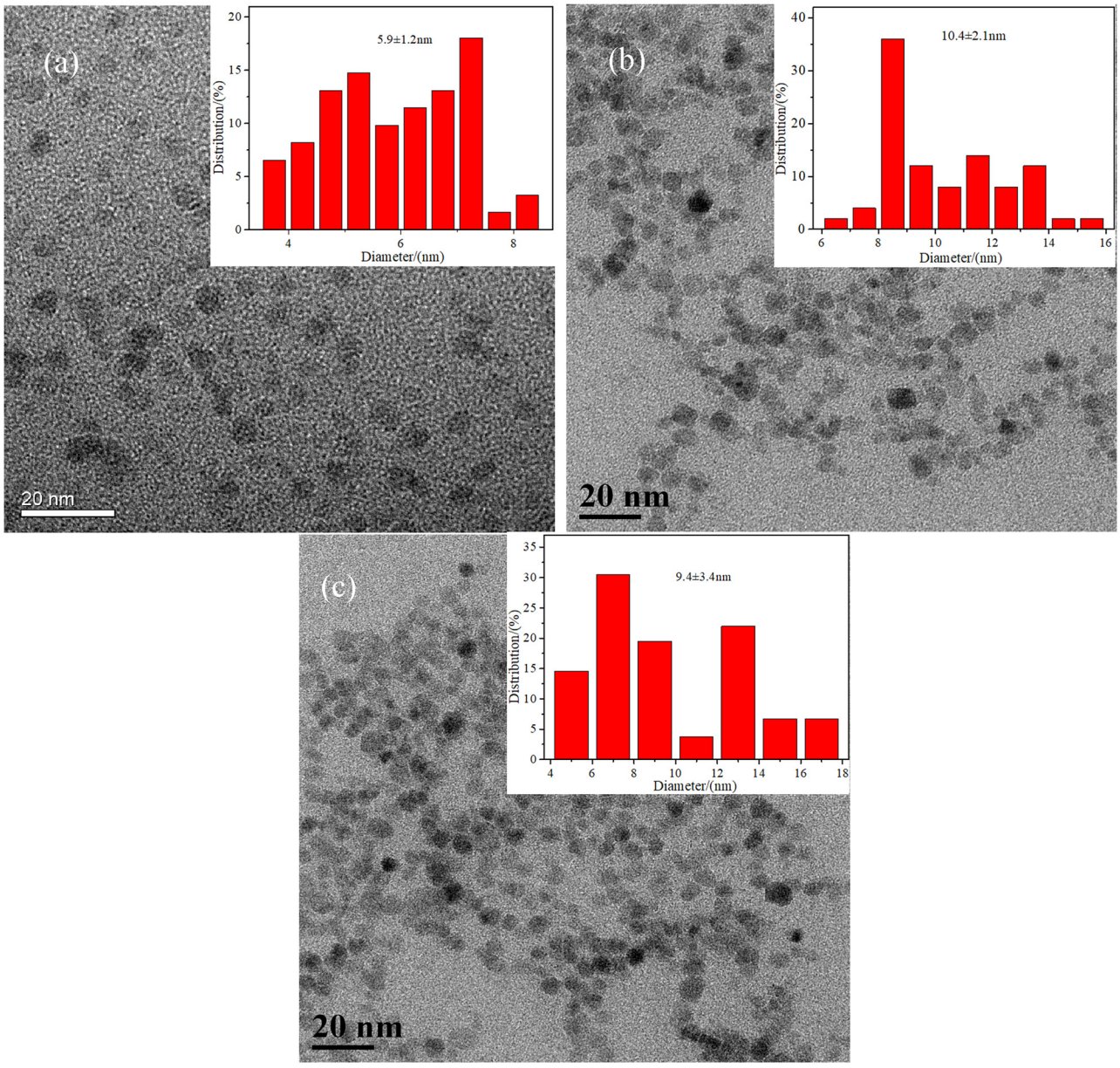

Figure 2: TEM images of Fe_3O_4@DDT-PMAA MF at (a) 0.5% of DDT-PMAA; (b) 1% of DDT-PMAA; and (c) 2% of DDT-PMAA, the scale bars are all in 20 nm.

NPs [25]. With the increase in the molar ratio of chain initiator DDT, the molecular weight fraction of DDT-PMAA decreased. That is, the chain length of the polymer became shorter, and the number of carboxylic acid functional groups decreased accordingly. Therefore, more polymers were needed when carboxyl groups coordinated with magnetic spheres, and more polymers were in the outermost layer of NPs, resulting in larger NPs [26,27]. Based on this, we chose 0.5% of DDT-PMAA as a surfactant for preparing MF by high-temperature co-precipitation to prepare super-small magnetic NPs.

3.1.2 Influence of molar ratio between DDT-PMAA and Fe_3O_4 on particle size

The amount of surfactant DDT-PMAA was an important factor affecting the size of NPs [28]. The control variable method was used to determine the effect of mass ratio between 0.5% of DDT-PMAA and Fe_3O_4, while maintaining the reaction temperature at 105°C and reaction time of 2 h. The size change in Fe_3O_4@DDT-PMAA magnetic NPs was investigated under different mass ratios (5:1, 10:1, 15:1, 20:1, and 25:1). We prepared a series of

products according to the molar ratio of Fe^{2+} to DDT-PMAA, and the other operations were similar to Section 2.3. The hydrodynamic diameter distributions and TEM images are shown in Figures S1 and S2.

It can be seen from Figure S1(a)–(e) that as the mass ratio of the polymer DDT-PMAA to Fe_3O_4 increased, the hydrodynamic diameter distribution of the magnetic NPs changed greatly. When the mass ratio of polymer DDT-PMAA to Fe_3O_4 were 5:1 and 10:1, the obtained magnetic NPs had a wide hydrodynamic diameter distribution and the average hydrodynamic diameter reached to 38.2 nm (PDI = 0.60) and 44.9 nm (PDI = 0.54), respectively. When the mass ratio was 15:1, the particle size distribution was narrow and the average hydrodynamic diameter was reduced to 15.7 nm (PDI = 0.23). When the mass ratio was increased to 20:1, the average hydrodynamic particle size of the magnetic NPs was only 1.6 nm (PDI = 0.28), but the particle size distribution did not conform to the normal distribution and the second peak of the particle size distribution had appeared, which indicated that the size distribution of the prepared magnetic NPs was not uniform. And when the mass ratio was 25:1, the obtained hydrodynamic diameter distribution of the magnetic NPs was similar to that of mass ratio of 20:1, and there were other peaks near 20–40 nm (PDI = 0.32). This showed that the content of DDT-PMAA had a great influence on the particle size, and when the ratio was 15:1, the effect was the best.

The morphology and particle size of the NPs in the prepared Fe_3O_4@DDT-PMAA MF can be clearly seen from Figure S2. It can be observed that when the mass ratio of polymer DDT-PMAA to Fe_3O_4 was 10:1, the obtained NPs were approximately spherical, and there was agglomeration among the NPs, with poor dispersion, and the average particle size was about 10.5 ± 2.8 nm. When the mass ratio was 5:1, 20:1, and 25:1, the prepared NPs had a relatively clear spherical profile, and the agglomeration phenomenon was slightly improved with better particle dispersion. The particle sizes were 6.4 ± 1.6, 5.9 ± 1.2, and 6.7 ± 1.6 nm, respectively. But the particle size distribution did not conform to the normal distribution, indicating that the particle size distribution was wide at this time. When the mass ratio was 15:1, the NPs showed a relatively clear spherical profile without the agglomeration phenomenon, and the particle size was 6.3 ± 1.3 nm, which was consistent with the above TEM results. Based on the hydrodynamic diameter distribution and TEM images of the NPs, it can be seen that the optimal mass ratio of the polymer DDT-PMAA to Fe_3O_4 was 15:1.

The particle size of the Fe_3O_4@DDT-PMAA NPs with different ratios of the polymer DDT-PMAA was different because the concentration of the carboxylic acid functional groups in the solution was different after the different amounts of the surfactants are dissolved. When the surfactant DDT-PMAA was less, the concentration of carboxylic acid in the solution was small [29], making the Fe_3O_4 magnetic NPs not completely covered by the modifier. The bare vacancies on the surface of the NPs were magnetically attracted, which resulted in an agglomeration of some NPs and the increase in the average particle diameter size. When the mass ratio of polymer DDT-PMAA to Fe_3O_4 was too large, the concentration of carboxylic acid in the solution was too high, exceeding the amount of reaction with Fe_3O_4 magnetic NPs, and the excess polymer was entangled with each other due to its long chain, which also made Fe_3O_4@DDT-PMAA NP size to increase [30]. So, a suitable DDT-PMAA to Fe_3O_4 mass ratio was especially important for the preparation of smaller size Fe_3O_4@DDT-PMAA MF.

3.1.3 Influence of reaction temperature on particle size

The reaction temperature directly affected the particle size and particle size distribution of Fe_3O_4@DDT-PMAA magnetic NPs, which was one of the important factors that need to be explored in this study [25]. For this purpose, the control variable method was used to control the reaction temperature of 95, 105, and 115°C under the premise of controlling the mass ratio of 0.5% of DDT-PMAA to Fe_3O_4 to 15:1 and reaction time of 2 h. The hydrodynamic diameter distribution and morphology of the prepared polymer DDT-PMAA-modified Fe_3O_4 NPs are shown in Figures S3 and S4, respectively.

It can be seen from Figure S3 that when the reaction temperatures were 95 and 105°C, the hydrodynamic diameter distributions of Fe_3O_4@DDT-PMAA magnetic NPs were narrow, and the average hydrodynamic diameters were 17.1 nm (PDI = 0.23) and 15.7 nm (PDI = 0.20), respectively. When the reaction temperature was increased to 115°C, the hydrodynamic diameter distribution of Fe_3O_4@DDT-PMAA magnetic NPs became wider, and the average hydrodynamic diameter was 17.3 nm (PDI = 0.56).

It can be seen from Figure S4 that the obtained NPs were spherical with clear contour, and there was almost no agglomeration among the NPs, exhibiting an outstanding dispersion. These NPs had a small average particle size of 6.2 ± 1.2, 5.9 ± 1.2, and 6.0 ± 1.1 nm at different temperatures (95, 105, and 115°C), respectively. The hydrodynamic diameter distribution and TEM images of the NPs showed that when the reaction temperature was

105°C, the obtained Fe_3O_4@DDT-PMAA MF exhibited great dispersibility, small particle size, and uniformity.

The main reason for this phenomenon was that temperature affected the nucleation and growth rate of NPs. When the reaction temperature was 95 and 105°C, the nucleation rate of Fe_3O_4 magnetic NPs was appropriate, and the generated NPs can react with surfactants in time. The growth of the NPs was inhibited to some extent, so the particle size distribution was narrow and the particle size was small. When the reaction temperature rose to 115°C, the nucleation rate of Fe_3O_4 magnetic NPs increased, and the Brownian motion of the particles increased. As a result, some of the NPs were accelerated, reacting with the surfactant in time and attracting each other to form a bigger core, so the particle size increases [25]. In conclusion, the optimal reaction conditions were as follows: 0.5% of DDT-PMAA was selected as the outer layer; the molar ratio of DDT-PMAA to Fe_3O_4 was 15:1; the reaction temperature was 105°C and the reaction time was 2 h. Under these optimal conditions, the average particle size was uniform (5.9 ± 1.2 nm) without aggregation and the hydrodynamic diameter was 15.7 nm (PDI = 0.20) with narrow distribution.

3.2 Characterization of Fe_3O_4@DDT-PMAA MFs

The preparation conditions of Fe_3O_4@DDT-PMAA MF by high temperature co-precipitation method were studied in the Section 3.1. The Fe_3O_4@DDT-PMAA water-based MF prepared under this condition will be characterized by FTIR, Raman, TGA, XRD, and XPS, so as to verify the correctness of the prepared MF; the details are as follows.

First of all, FTIR was used to characterize the prepared NPs to determine the chemical structure of the sample surface. In Figure 3a, the black line is the infrared spectrum of bare Fe_3O_4 magnetic NPs. The absorption peaks at wavelengths of 3,318 and 1,633 cm^{-1} were generated by surface hydroxyl groups and water molecules, respectively. The wavelength of 550 cm^{-1} represented the characteristic peak of the Fe-O functional group. In Figure 3a,, it can be observed from the blue line that there was a strong absorption peak at a wavelength of 1,713 cm^{-1} due to the asymmetric stretching of the carbonyl group (–CO–) in the polymer molecule. As a result, this absorption peak of Fe_3O_4@DDT-PMAA magnetic NPs was somewhat weakened, shown in red line in Figure 3a [31]. At the same time, the absorption peaks of 1,390 and 1,488 cm^{-1} represented the stretching vibration of the carboxylic acid in the polymer DDT-PMAA, and the two absorption peaks were located at 1,207 and 1,453 cm^{-1} in Fe_3O_4@DDT-PMAA magnetic NPs. The polymer DDT-PMAA and Fe_3O_4@DDT-PMAA NPs had an absorption peak around 3,300 cm^{-1}, which was caused by the stretching vibration of the carboxylic acid O–H in the polymer DDT-PMAA [32]. The Fe_3O_4@DDT-PMAA NPs had an absorption peak at 595 cm^{-1}, which was attributed to the stretching vibration of Fe–O, which was only present in Fe_3O_4 magnetic NPs and Fe_3O_4@DDT-PMAA magnetic NPs [33]. Through the comparative analysis of the infrared spectrum, it can be proved that the polymer DDT-PMAA existed on the surface of Fe_3O_4 magnetic NPs and the modification was successful.

It is not possible to accurately determine whether the NPs are Fe_3O_4 or Fe_2O_3 only by FTIR characterization method, because the two characterization methods (TEM and FTIR) were not sensitive to the determination of iron oxide, resulting in a certain degree of deviation in the test results. Therefore, it was necessary to carry out a deeper test on the prepared magnetic NPs by Raman spectroscopy to determine whether the particles are Fe_3O_4 or Fe_2O_3. In this study, the Raman spectrum of the polymer DDT-PMAA-modified magnetic NPs is shown in Figure 3b. As can be seen from the Figure 3b, a strong peak appears at a wavelength of 665 nm, which indicated that the main phase of the iron oxide was Fe_3O_4 [34].

In order to further prove that the core of the NPs is Fe_3O_4, we used XPS to characterize it, as shown in Figure 3c–d. From Figure 3c, We can clearly see the corresponding fitting curves of C 1s, O 1s, and Fe 2p, which again prove the existence of DDT-PMAA in the cladding and the core-shell structure [35]. Similarly, we observed that the binding energy values of Fe $2p_{3/2}$ and Fe $2p_{1/2}$ were 710.8 ad 724.6 eV, respectively in Figure 3d, corresponding to the previous reports about Fe_3O_4 NPs [36]. In addition, the characteristic absorption peak of γ-Fe_2O_3 was absent at 719.0 eV, which further proved that the NPs were Fe_3O_4 NPs.

Similarly, the crystal form of NPs had a certain influence on the stability and magnetic properties of MF [37]. Therefore, XRD was used to detect the crystal form, as shown in Figure 3e. The characteristic diffraction peaks at 30.0°, 35.5°, 43.0°, 53.0°, 57.0°, and 62.6° observed from the XRD patterns belong to (220), (311), (400), (422), (511), and (440) planes of the samples, respectively, which were consistent with the inverse cubic spinel phases of Fe_3O_4 (JCPDS card No. 75-1609) [38]. It can be seen from the XRD patterns of the DDT-PMAA coated Fe_3O_4 that the position of the major peaks does not change, in other words, the crystal phase of the Fe_3O_4 NPs does not change after coating.

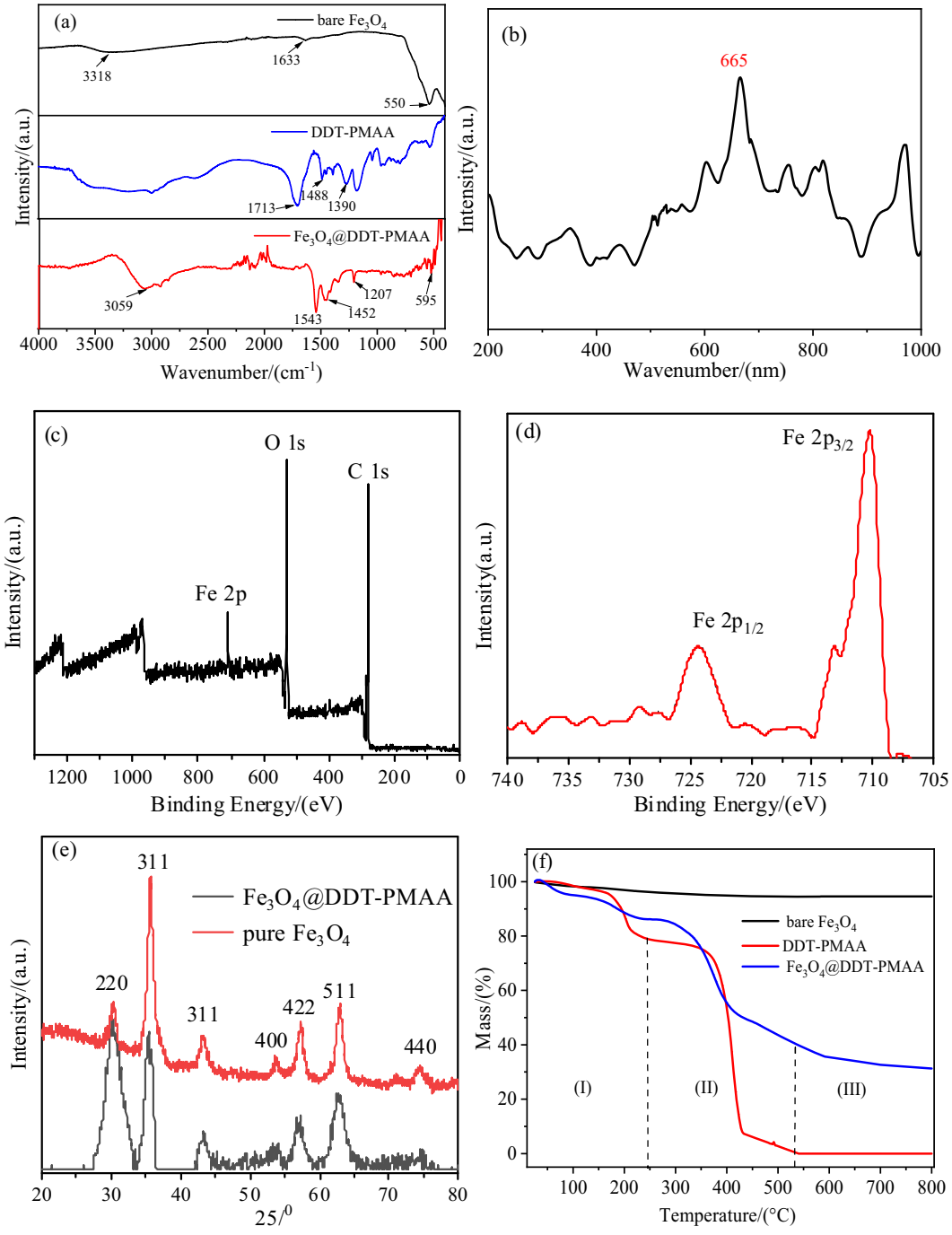

Figure 3: Different characterizations for Fe_3O_4@DDT-PMAA MFs, (a) FTIR spectra of bare Fe_3O_4, DDT-PMAA, and Fe_3O_4@DDT-PMAA; (b) Raman spectra of Fe_3O_4@DDT-PMAA NPs under N_2 protection; (c and d) XPS survey spectrum of Fe_3O_4@DDT-PMAA; (e) TGA curves of DDT-PMAA, bare Fe_3O_4, and Fe_3O_4@DDT-PMAA magnetic NPs under N_2 protection; and (f) XRD for bare Fe_3O_4 and Fe_3O_4@DDT-PMAA.

In order to further investigate the thermal stability of the prepared Fe_3O_4@DDT-PMAA magnetic NPs and to calculate the content of polymer DDT-PMAA and Fe_3O_4 NPs in the modified magnetic NPs, TGA under nitrogen protection was performed for DDT-PMAA, unmodified Fe_3O_4 magnetic NPs, and Fe_3O_4@DDT-PMAA magnetic NPs. The obtained weight loss curves are shown in Figure 3f.

It can be seen from Figure 3f that the weight loss curve of the unmodified Fe_3O_4 magnetic NPs was relatively smooth, and the sample quality was slightly reduced,

which was caused by the evaporation of a small amount of water on the surface of the NPs. In the test temperature range, the Fe_3O_4 NPs did not decompose. The weight loss of the polymer DDT-PMAA before 200°C was relatively slow, which was mainly due to the evaporation of surface moisture. When the temperature rose to 380°C, the weight of the polymer decreased sharply, which indicated that the polymer began to decompose. At 539°C, the weight of the polymer DDT-PMAA was reduced to zero and the sample was completely decomposed. The weight loss curve of Fe_3O_4@DDT-PMAA magnetic NPs can be divided into three stages: the first stage (I) was the temperature of Fe_3O_4@DDT-PMAA magnetic NPs, which was between room temperature and 200°C. The loss mainly came from the evaporation of water adsorbed on the surface of the NPs; the second stage (II) of weight loss was due to the increase in temperature from 380 to 539°C. This part of the weight loss was less, which was mainly due to the decomposition of polymer DDT-PMAA on the magnetic NPs surface, which also proved that the polymer DDT-PMAA had been successfully coated on the surface of Fe_3O_4 magnetic NPs. After the polymer DDT-PMAA was completely decomposed, the remaining was mainly Fe_3O_4 magnetic NPs. Therefore, the weight of Fe_3O_4@DDT-PMAA magnetic NPs hardly changed when the temperature was more than 539°C which is the third stage (III). According to the weight loss curve, the mass ratio (wt%) of the polymer DDT-PMAA and Fe_3O_4 in Fe_3O_4@DDT-PMAA magnetic NPs can be calculated to be 64.7 and 35.3%, respectively. In conclusion, we had successfully prepared DDT-PMAA coated Fe_3O_4 NPs.

3.3 Stability of Fe_3O_4@DDT-PMAA MFs

The stability of the prepared Fe_3O_4@DDT-PMAA MF in an external magnetic field and acid–base salt environment was the prerequisite for being used as a magnetic resonance contrast agent. Therefore, the stability of the MF had been investigated in detail.

The static stability of the Fe_3O_4@DDT-PMAA nanomagnetic fluid was expressed by the stability index (I). The density, stability index, and duration time of the fresh and timed Fe_3O_4@DDT-PMAA MF were determined by densitometer. The stability index I was calculated as follows:

$$I = \frac{\rho_s - \rho_w}{\rho - \rho_w},$$

where ρ and ρ_s represent the initial density of the sample and the density that changes with time (kg m^{-3}), respectively, and ρ_w represents the water density (kg m^{-3}). The relationship is shown in Figure 4a. The stability index of Fe_3O_4@DDT-PMAA MF did not change within 90 days, indicating that the prepared MF had excellent stability. Besides, no obvious aggregation and precipitation can be observed after 120 days' storage at room temperature (Figure S5), indicating that the prepared Fe_3O_4@DDT-PMAA MF had a good stability.

Similarly, the magnetic stability of Fe_3O_4@DDT-PMAA MF was measured by Gouy magnetic balance. The magnetic weight of Fe_3O_4@DDT-PMAA MF was observed under an external magnetic field of 40 mT. It can be seen from Figure 4b that the magnetic weight of the Fe_3O_4@DDT-PMAA MF was stable at a value of about 40 mT. Since the

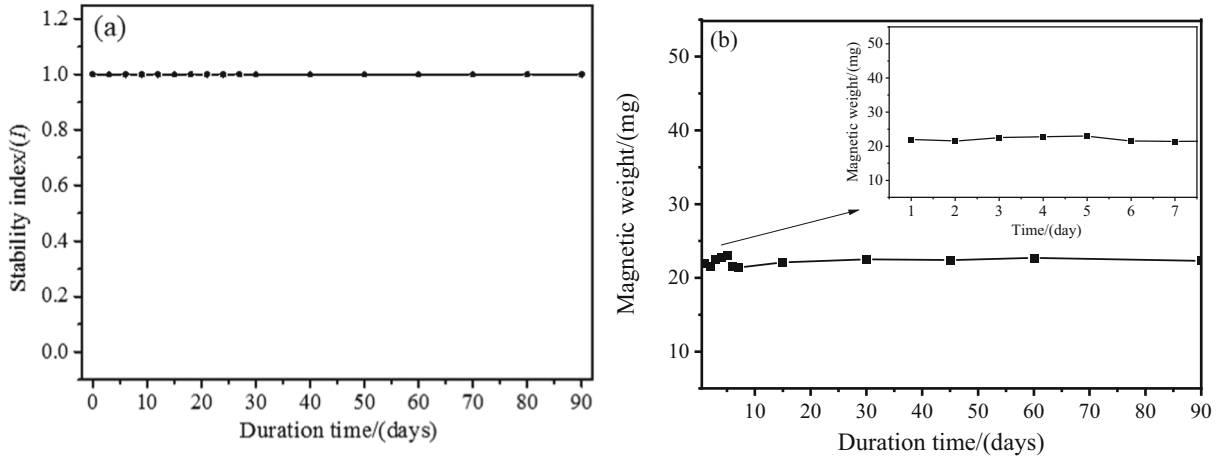

Figure 4: Stability characterization of Fe_3O_4@DDT-PMAA MFs, (a) stability index *versus* duration time and (b) relationship between time and increased magnetic weight in magnetic field of 40 mT.

applied magnetic field was not uniform, the magnetic weight of MF hardly changed, indicating that it had a certain magnetic field.

3.3.1 Stability of Fe_3O_4@DDT-PMAA MFs at different pH

Equal concentrations of Fe_3O_4@DDT-PMAA MF samples were placed in 5 mL tubes, and the pH of Fe_3O_4@DDT-PMAA MF was adjusted to 1–14, respectively, using hydrochloric acid and NaOH solution. We observed the change in the sample in different acid–base environments storing for 60 days. As presented in Figure 5, it showed that the Fe_3O_4@DDT-PMAA MF completely decomposed at pH = 1 and the solution was yellow which was the color of Fe^{3+}. At pH = 2, 3, and 4, a small amount of NPs precipitated. Compared with the acidic environment, the MF was more stable in an alkaline environment, and there was only a

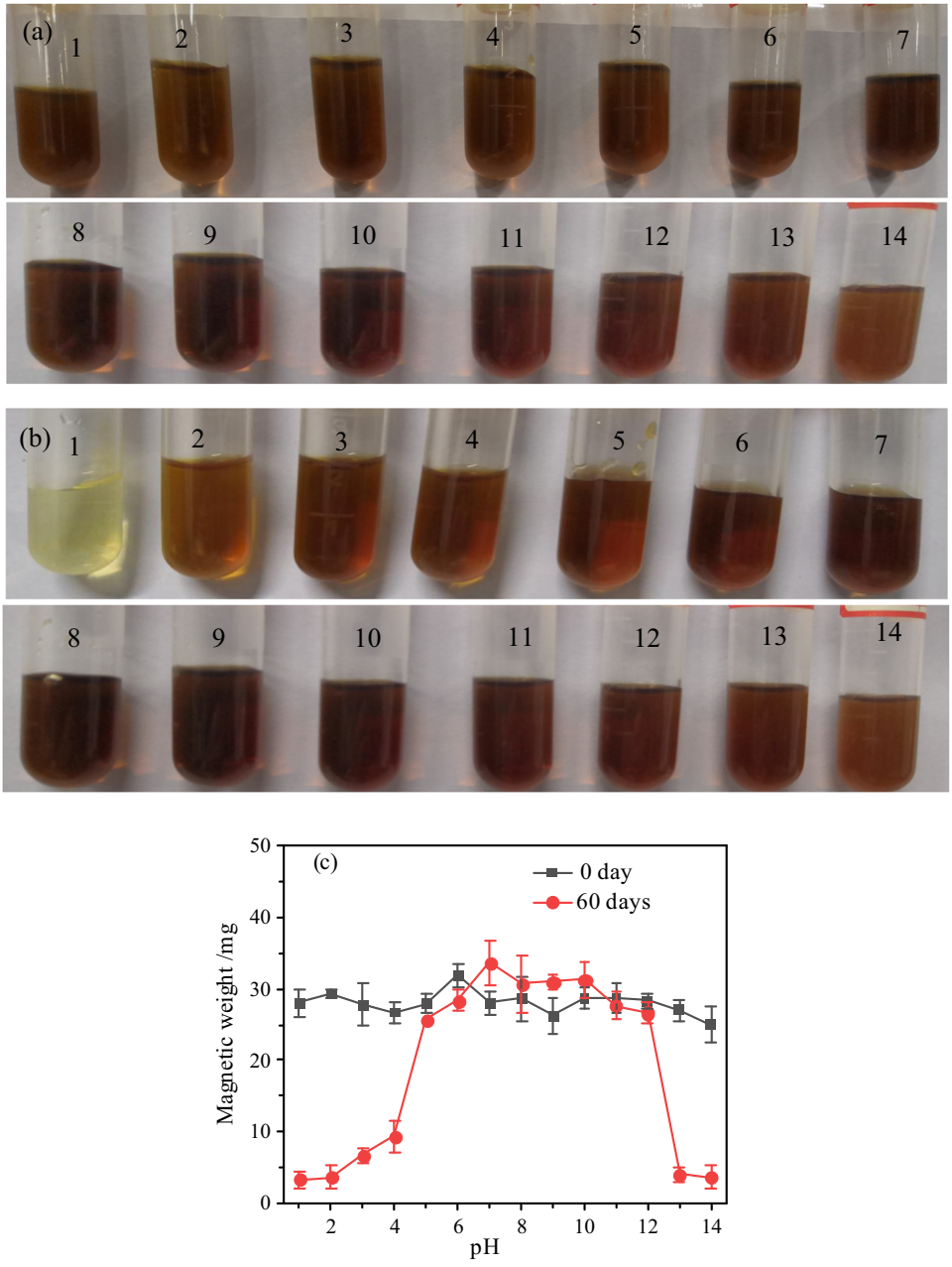

Figure 5: Stability change in Fe_3O_4@DDT-PMAA MF in different pH environments for different time, (a) photos for 0 day; (b) photos for 60 days; and (c) magnetic gain in 60 days with 40 mT.

little precipitation at pH 13 and 14. Overall, the Fe_3O_4@DDT-PMAA MF had good stability in an environment with a pH of 5–12.

In order to further visualize the stability of MF under different pH values, this study used the change in magnetic weight gain to show the change in the stability in detail. From Figure 5c, it can be clearly seen that the change in the magnetic gain was basically maintained at about 30 mg within 0 days; At 60 days, the magnetic gain of samples with pH less than 5 and more than 12 was less than 10 mg, which was mainly due to the decomposition of Fe_3O_4 NPs caused by strong acid, and the precipitation of MF caused by strong alkali, so the magnetic properties were reduced. More importantly, it was consistent with the results of Figure 5a and b.

3.3.2 Stability of Fe_3O_4@DDT-PMAA MFs in salt solution

Equal concentrations of Fe_3O_4@DDT-PMAA MF were placed in small tubes and then different concentrations of NaCl solution were added to the tubes. The concentrations of NaCl solution were 0.1, 0.25, 0.5, 0.75, 1.0, 1.25, 1.5, 1.75, and 2.0 mol L^{-1}, respectively. The MF dispersed in the salt solution was stored at room temperature for 60 days to observe the stability. It can be seen from the Figure S6a and b that Fe_3O_4@DDT-PMAA MF had no particle precipitation in different concentrations of salt solution, which preliminary indicated that the prepared Fe_3O_4@DDT-PMAA MF owned great salt solution stability. In Figure S6c, we can clearly see that: (i) under different salt concentrations, the magnetic gain was basically maintained at about 30 mg; (ii) within 60 days, the magnetic gain was also basically stable at 30 mg; and the most important thing was consistent with Figure S6(a) and (b). To sum up, it proved that the MF showed excellent long-term stability (60 days), even if the salt concentration was as high as 2 mol L^{-1}.

3.3.3 Zeta potential of Fe_3O_4@DDT-PMAA MFs

Zeta potential analysis can be used to indicate the charge and stability of the NPs in the base carrier. The larger the zeta potential value is, the more charge on the surface of the NPs, and the more stable it would be in the base carrier. When the zeta potential value exceeded 61 mV, the MF had excellent stability [39]. From Figure 6, the unmodified Fe_3O_4 MF had a potential of –16.2 mV, and the zeta potential of the MF modified by the polymer

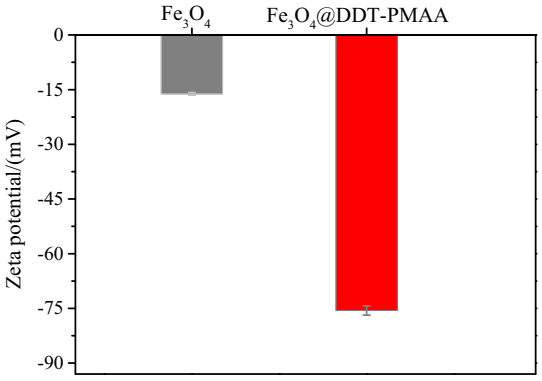

Figure 6: Zeta potential of uncoated and Fe_3O_4@DDT-PMAA magnetic NPs in water (pH = 7).

DDT-PMAA became –75.6 mV. This was because the surface of the surfactant DDT-PMAA contained a large number of carboxyl groups, which also proved that the polymer DDT-PMAA was successfully modified on the Fe_3O_4 magnetic NPs. The prepared Fe_3O_4@DDT-PMAA MF had a large negative zeta potential, good electrostatic stability in the base carrier liquid, and good polymer repulsion at the same time. Moreover, relative to the spatial repulsion, the stronger the electrostatic interaction between the particles (the larger the zeta potential value) is, the more stable the MF will be, which proved that the Fe_3O_4@DDT-PMAA MF samples possessed very great stability.

3.4 Dual-model MRI of Fe_3O_4@DDT-PMAA MFs

3.4.1 *In vitro*

Magnetic saturation strength (M_s), longitudinal relaxation (r_1), and transverse relaxation (r_2) were used to evaluate the effect of *in vitro* imaging. As presented in the Figures S7 and S8, the *M*s of the pure Fe_3O_4 magnetic NPs was 66.39 emu g^{-1}, and the initial magnetic susceptibility was very high, while the *M*s of the Fe_3O_4@DDT-PMAA MFs was reduced to 15.73 emu g^{-1}, and the initial magnetic susceptibility was correspondingly reduced. There were two reasons for this result. One was that the magnetic NP surface was introduced with the non-magnetic substance DDT-PMAA, and the other was that the M_s of the particles had a great relationship with the size of the NPs, while the modified NPs owned a particle size of only 5.9 nm and the magnetic moment was very small [40].

Fe_3O_4 magnetic NPs with super-small particle sizes showed great potential in T_1 and T_2 signal magnetic contrast agents. *In vitro* T_1 and T_2 mapping imaging of Fe_3O_4@DT-PMAA MFs were measured by a clinical Siemens 3.0 T magnetic resonance scanner. The value of r_1 and r_2 directly measured the imaging effect. From Figure 7, it can be seen that the intensity of the T_1 and T_2 signals had a great relationship with the concentration of Fe in the MF. With the increase in Fe concentration in the Fe_3O_4@DDT-PMAA MF, the T_1 and T_2 signals were constantly enhanced. The measured intensity was plotted against the Fe concentration in the MF, and the resulting map was linearly fitted, as shown in Figure 7c. The value of r_1 and r_2 (Here 1 and 2 are subscript to *r*) were 6.9 and 43.7 $mM^{-1} s^{-1}$, respectively, which was approximately 2.38 times that of the commercial contrast agent SHU-555C (the composition was carboxydextran-coated Fe_3O_4, the *d*hyd/*d*TEM values were 20 and 5 nm, r_1 = 2.9 $mM^{-1} s^{-1}$) and accounted for 64.5% of the commercial contrast agent Feridex (the composition was dextran T10-coated mixture Fe_3O_4 and Fe_2O_3, the *d*hyd/*d*TEM values were 4.8 and 58.5 nm, r_2 = 67.8 $mM^{-1} s^{-1}$) [41]. The key reason for the high r_1 value was the super-small size of NPs (5.9 nm), which can significantly improve the longitudinal relaxation and weaken the transverse relaxation [42]. Similarly, it is one of the reasons for the decrease in r_2 value, that is, the increase in specific surface area led to the surface spin tilt effect, and the surface disorder increased, resulting in magnetic weakening [43]. Another important reason for the lower r_2 value was the lower *M*s (15.73 emu g^{-1}), which was directly related to the strength of r_2 value [25]. Based on the above results, the Fe_3O_4@DDT-PMAA MFs showed great potential in magnetic contrast T_1 and T_2 signals.

3.4.2 *In vivo*

The liver as the region of interest was selected for observation pre-and post-injection of Fe_3O_4@DDT-PMAA MFs at a low dose (0.8 mg Fe kg^{-1}) in transverse and longitudinal imaging. The T_1-weighted images became brighter and T_2-weighted images became darker when compared with the T_1 and T_2-weighted pre-contrast images (Figure 8). It can be clearly seen from the comparison of Figure 8a and b that the bright visual field increased significantly, where the area was not clear before injection was clearly visible after injection (in the red circle, hepatoma cells), in addition, other tissues were clearly visible (in the blue circle), which was mainly related to the higher r_1 value [44]. Furthermore, the background of Figure 8b was less visible, which may be related to the drug metabolism mainly in the liver. Similarly, T_2-maping imaging had similar results, the picture was clearer and the tissue was more obvious. More importantly, the background image became more blurred after administration than before, which indicated that it was more helpful for accurate diagnosis after administration. The results showed that Fe_3O_4@DDT-PMAA MFs owned the potential for simultaneous T_1 and T_2 contrast enhancement images, which can provide more comprehensive information

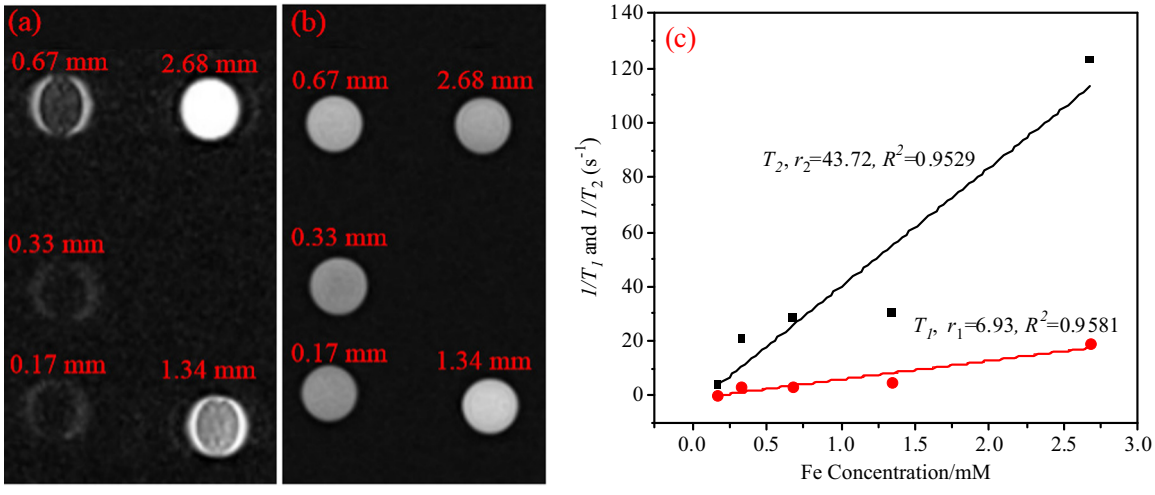

Figure 7: T_1 and T_2 mapping images of different concentrations of Fe_3O_4@DDT-PMAA MF *in vitro*, (a) T_1 mapping images, (b) T_2 mapping images, and (c) T_1 longitudinal and T_2 transverse relaxivity with different Fe concentrations.

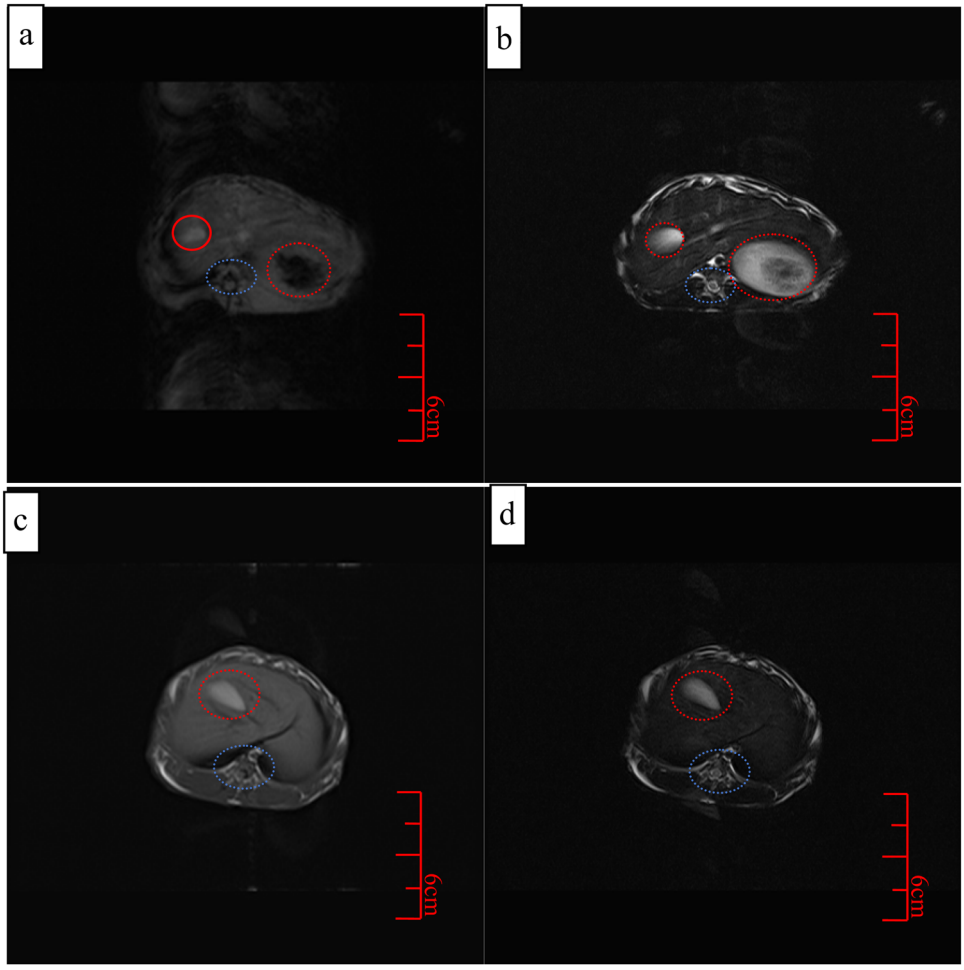

Figure 8: Simultaneous T_1- and T_2-weighted coronal images of Fe_3O_4@DDT-PMAA MFs in rabbit liver cancer, (a) pre-rejection for T_1 images; (b) after-rejection for T_1 images; (c) pre-rejection for T_2 images; and (d) after-rejection for T_2 images.

and higher accuracy for image-guided diagnosis and treatment.

4 Conclusion

In this article, polymer DDT-PMAA was used as a surfactant to prepare MF with a particle size of only 5.9 nm by high temperature chemical co-precipitation. The influencing factors of the preparation of super-small-diameter magnetic NPs were investigated in depth. Under the optimal preparation conditions, the water-based MF with super-small particles was successfully prepared and modified by polymer DDT-PMAA. The particles' diameter distribution is narrow and uniformly dispersed, and there is almost no agglomeration. The magnetic NPs have a regular shape which is approximately spherical and has a clear outline. Moreover, because the particle size is small, the corresponding saturation magnetization is also reduced. The prepared Fe_3O_4@DDT-PMAA MF exhibits excellent stability and can stably exist in magnetic field, acid–base environment, and salt solution, which is closely related to the higher zeta potential (−75.59 mV) and the super-small particle size of MF. Simultaneously, the MRI effect is more vivid and there is almost no background interference *in vivo*, though the value of r_2 is slightly lower than commercial contrast agents *in vitro*. In conclusion, the prepared Fe_3O_4@DDT-PMAA MF possesses small size and good stability, exhibiting an excellent comprehensive performance, and shows great development potential as magnetic contrast agent in T_1 and T_2 dual-mode MRI. In the future, we will do more detailed research on reducing toxicity and improving sensitivity, and the drug metabolism and pharmacokinetics *in vivo* should be discussed accordingly. At the same time, the optimization of reaction conditions is emphasized to facilitate industrial production.

Funding information: This research was financially supported by the National Natural Science Foundation of China (NSFC, No. 21246002), Minjiang Scholarship of Fujian Province (No. in-Gaojiao[2010]-117), Central-government Guided Fund for Local Economic Development (No. 830170778), R&D Fund for Strategic Emerging Industry of Fujian Province (No. 82918001), and International Cooperation Project of Fujian Science and Technology Department (No. 830170771).

Author contributions: All authors have accepted responsibility for the entire content of this manuscript and approved its submission.

Conflict of interest: The authors state no conflict of interest.

References

[1] Yang LJ, Sun CJ, Lin HY, Gong XS. Sensitive contrast-enhanced magnetic resonance imaging of orthotopic and metastatic hepatic tumors by ultralow doses of zinc ferrite octapods. Chem Mate. 2019;31(4):1381–90.

[2] Wang BC, Wu HH, Xu PP, Xu PP, Jiang P, Xia GL, et al. Core-shell structurized Fe_3O_4@C@MnO_2 nanoparticles as pH responsive T1-T2* dual-modal contrast agents for tumor diagnosis. ACS Biomater Sci Eng. 2018;4:3047–54.

[3] Chen Y, Li M, Hong Y, Lam JWY, Zheng QC, Tang BZ. Dual-modal MRI contrast agent with aggregation-induced emission characteristic for liver specific imaging with long circulation lifetime. ACS Appl Mater Inter. 2014;6(13):10783–91.

[4] Li HC, Yang SQ, Hui D, Hong RY. Progress in magnetic Fe_3O_4 nanomaterials in magnetic resonance imaging. Nanotechnol Rev. 2020;9:1265–83.

[5] Yang L, Shao B, Zhang XT, Cheng Q, Lin T, Liu EZ. Multifunctional upconversion nanoparticles for targeted dual-modal imaging in rat glioma xenograft. J Biomater Appl. 2016;31(3):400–10.

[6] Zhou ZY, Chen HW, Lipowska M, Wang LY, Yu QQ, Yang XF, et al. A dual-modal magnetic nanoparticle probe for preoperative and intraoperative mapping of sentinel lymph nodes by magnetic resonance and near infrared fluorescence imaging. J Biomater Appl. 2013;28(1):100–11.

[7] Kim BH, Lee N, Kim H, An K, Park YI, Choi Y. Large-scale synthesis of uniform and extremely small-sized iron oxide nanoparticles for high-resolution T1 magnetic resonance imaging contrast agents. J Am Chem Soc. 2011;133:12624–31.

[8] Li JY, Yao M, Shao YX, Yao DF. The application of bio-nanotechnology in tumor diagnosis and treatment: a view. Nanotechnol Rev. 2018;7(3):257–66.

[9] Lee M, KimKuo YJ. Thermomagnetic convection of ferrofluid in an enclosure channel with an internal magnetic field. Micromachines. 2019;10(9):553.

[10] Rai M, Ingle-Avinash P, Pandit R, Priti P. Copper and copper nanoparticles: role in management of insect-pests and pathogenic microbes. Nanotechnol Rev. 2018;7(4):303–15.

[11] Jiang QL, Hong RY, Deng SM, Guo L, Hu RL, Gao B, et al. Folic acid-conjugated Fe_3O_4 magnetic nanoparticles for hyperthermia and MRI *in vitro* and *in vivo*. Appl Surf Sci. 2014;307:224–33.

[12] Yang Y, Qin Z, Zeng W, Ting Y. Toxicity assessment of nanoparticles in various systems and organs. Nanotechnol Rev. 2016;6(3):279–89.

[13] Gong Y, Dai JW, Li H, Wang X, Xiong HR, Zhang QY, et al. Magnetic, fluorescent, and thermo-responsive poly(MMA-NIPAM-Tb$(AA)_3$Phen)/Fe_3O_4 multifunctional nanospheres prepared by emulsifier-free emulsion polymerization. J Biomater Appl. 2015;30(2):201–11.

[14] Fratantonio D, Marcos RC, Christine B, Lucien B. Stéphane Colin. Velocity measurements in channel gas flows in the slip regime by means of molecular tagging velocimetry. Micromachines. 2020;11:374.

[15] Hu FQ, Jia QJ, Li YL, Gao MY. Facile synthesis of ultrasmall PEGylated iron oxide nanoparticles for dual-contrast T-1- and T-2-weighted magnetic resonance imaging. Nanotechnol. 2011;22(24):245604.

[16] McNamara K, Tofail SA. Nanosystems: the use of nanoalloys, metallic, bimetallic, and magnetic nanoparticles in biomedical applications. Phys Chem Chem Phys. 2015;17:27981–95.

[17] Liu D, Wu W, Ling J, Wen S, Gu N, Zhang X. Effective PEGylation of iron oxide nanoparticles for high performance *in vivo* cancer imaging. Adv Funct Mater. 2011;21:1498–504.

[18] Wu W, He Q, Jiang C. Magnetic iron oxide nanoparticles: synthesis and surface functionalization strategies. Nanoscale Res Lett. 2008;3(11):397–415.

[19] Libi S, Calenic B, Astete CE, Kumar C, Sabliov CM. Investigation on hemolytic effect of poly(lactic co-glycolic) acid nanoparticles synthesized using continuous flow and batch processes. Nanotechnol Rev. 2019;6(2):209–20.

[20] Chanana M, Mao Z, Wang D. Using polymers to make up magnetic nanoparticles for biomedicine. J Biomed Nanotechnol. 2009;5(6):652–68.

[21] Li Z, Yi PW, Sun Q, Lei H, Zhao HL, Zhu ZH, et al. Ultrasmall water-soluble and biocompatible magnetic iron oxide nanoparticles as positive and negative dual contrast agents. Adv Funct Mater. 2012;22(11):2387–93.

[22] Zhang H, Huang X, Li L, Zhang G, Hussain I, Li Z, et al. Photoreductive synthesis of water-soluble fluorescent metal nanoclusters. Chem Commun. 2012;48:567–9.

[23] Xie J, Chen K, Lee HY, Xu CJ, Hsu AR, Peng S, et al. Ultrasmall c (RGDyK)-coated Fe_3O_4 nanoparticles and their specific targeting to integrin tumor cells. J Am Chem Soc. 2008;130:7542–3.

[24] Wang Z, Tan B, Hussain I, Schaeffer N, Wyatt MF, Brust M, et al. Design of polymeric stabilizers for size-controlled synthesis of monodisperse gold nanoparticles in water. Langmuir. 2007;23(2):885–95.

[25] Ali S, Khan SA, Yamani ZH, Qamar MT, Morsy MA, Sarfraz S. Shape- and size-controlled superparamagnetic iron oxide nanoparticles using various reducing agents and their relaxometric properties by Xigo acorn area. Appl Nanosci. 2019;9:479–89.

[26] Xie J, Xu C, Kohler N, Hou YL. Controlled PEGylation of monodisperse Fe_3O_4 nanoparticles for reduced non-specific uptake by macrophage cells. Adv Mater. 2007;19(20):3163–6.
[27] Majeed MI, Lu Q, Yan W, Hussain I. Highly water-soluble magnetic iron oxide (Fe_3O_4) nanoparticles for drug delivery: enhanced *in vitro* therapeutic efficacy of doxorubicin and MION conjugates. J Mater Chem B. 2013;1(22):2874–84.
[28] Kubovcikova M, Koneracka M, Strbak O, Molcan M, Zavisova V, Antal I, et al. Poly-L-lysine designed magnetic nanoparticles for combined hyperthermia, magnetic resonance imaging and cancer cell detection. J Magn Magn Mater. 2019;475:316–26.
[29] Kikuchi T, Kasuya R, Endo S, Nakamura A, Takai T, Nils MN, et al. Preparation of magnetite aqueous dispersion for magnetic fluid hyperthermia. J Magn Magn Mater. 2011;323(10):1216–22.
[30] Abareshi M, Goharshadi EK, Zebarjad SM, Fadafand HK. Fabrication, characterization and measurement of thermal conductivity of Fe_3O_4 nanofluids. J Magn Magn Mater. 2010;322(24):3895–901.
[31] Nawara K, Romiszewski J, Kijewska K, Szczytko J. Adsorption of doxorubicin onto citrate-stabilized magnetic nanoparticles. J Phys Chem C. 2012;116(116):5598–609.
[32] Sun L, Huang C, Gong T, Zhou SB. A biocompatible approach to surface modification: biodegradable polymer functionalized super-paramagnetic iron oxide nanoparticles. Mat Sci Eng C. 2010;30(4):583–9.
[33] Li Z, Tan B, Allix M, Cooper AI, Rosseinsky MJ. Direct coprecipitation route to monodisperse dual-functionalized magnetic iron oxide nanocrystals without size selection. Small. 2010;4(2):231–9.
[34] Testa-Anta M, Ramos-Docampo MA, Comesaña-Hermo M, Rivas-Murias B, Salgueiriño V. Raman spectroscopy to unravel the magnetic properties of iron oxide nanocrystals for bio-related applications. Nanoscale Adv. 2019;1:2086.
[35] Jing X, Zhi Z, Jin LM, Wang F, Wu YS, Wang DQ. pH/redox dual-stimuli-responsive cross-linked polyphosphazen nanoparticles for multimodal imaging-guided chemophotodynamic therapy. Nanoscale. 2019;11:9457.
[36] Wang GN, Zhang XJ, Skallberg A, Liu YX, Hu ZJ, Mei XF, et al. One-step synthesis of water-dispersible ultra-small Fe_3O_4 nanoparticles as contrast agents for T1 and T2 magnetic resonance imaging. Nanoscale. 2014;6:2953.
[37] Sun XN, Du RH, Zhang L, Zhang GL, Zheng XJ, Qian JC, et al. A pH-responsive yolk-like nanoplatform for tumor targeted dual-mode magnetic resonance imaging and chemotherapy. ACS Nano. 2017;11:7049–59.
[38] Shu RW, Wang M, Yang YY, Chang SY, Zhang GY, Gan Y, et al. Solvothermal synthesis of reduced graphene oxide/ferroferric oxide hybrid composites with enhanced microwave absorption properties. Nano. 2017;12(12):21–33.
[39] Araújo-Neto RP, Silva-Freitas EL, Carvalho JF, Pontes TRF, Silva KL, Damasceno IHM, et al. Monodisperse sodium oleate coated magnetite high susceptibility nanoparticles for hyperthermia applications. J Magn Magn Mater. 2014;364:72–9.
[40] Pichon BP, Barbillon G, Marie P, Matthias P, Sylvie BC. Iron oxide magnetic nanoparticles used as probing agents to study the nanostructure of mixed self-assembled monolayers. Nanoscale. 2011;3(11):4696–705.
[41] Yin JC, Xu FH, Qu HB, Li CR. Dysprosium-doped iron oxide nanoparticles boosting spin-spin relaxation: a computational and experimental study. Phys Chem Chem Phys. 2019;21:11883–92.
[42] Yang TG, Niu D, Chen JZ, He JP, Yang SB, Jia XB, et al. Biodegradable organosilica magnetic micelles for magnetically targeted MRI and GSH-triggered tumor chemotherapy. Biomater Sci. 2019;7:2951–60.
[43] Miao Yd, Xie FN, Cen JY, Zhou F, Tao XF, Luo JF, et al. Fe^{3+} @polyDOPA-b-polysarcosine, a T1-weighted MRI contrast agent via controlled NTA polymerization. ACS Macro Lett. 2018;7:693–8.
[44] Guldris N, Barbara A, Juan G, Ramon IR, Enrique CA, Yury VK, et al. Magnetite nanoparticles for stem cell labeling with high efficiency and long-term *in vivo* tracking. Bioconjugate Chem. 2017;28:362–70.